



## Original Article

## Nacre-like alumina with unique high strain rate capabilities

Koen Evers<sup>a,\*</sup>, Simone Falco<sup>b</sup>, Nicole Grobert<sup>a,c</sup>, Richard I. Todd<sup>a</sup><sup>a</sup> Department of Materials, University of Oxford, Parks Road, Oxford, OX1 3PH, UK<sup>b</sup> Department of Engineering Science, University of Oxford, Parks Road, Oxford, OX1 3PJ, UK<sup>c</sup> Williams Advanced Engineering, Grove, Oxfordshire, OX12 0DQ, UK

## ARTICLE INFO

## Keywords:

Biomimicry

Alumina

Nacre

SPS

High strain rate

## ABSTRACT

Nacre-like alumina manufactured using spark plasma sintering shows a strikingly different mechanical behaviour compared to conventional alumina. A range of sintering conditions were applied to micron-sized alumina platelet powders to form alumina with different nacre-like microstructures, density, grain size and flexural strength. We show that a microstructure of aligned sintered platelets not only mitigates the typical issue of brittleness, but also has extraordinary energy absorption capabilities. It can withstand an impact with up to three times the kinetic energy required to break monolithic alumina while maintaining structural integrity. The high-rate compressive strength is shown to be more than 50% higher than that of monolithic alumina and we show energy absorption mechanisms such as crack deflection and branching to be present. Our approach provides a fast and effective way of manufacturing aligned nacre-like ceramic microstructures that maintain structural integrity through energy dissipation and interlocking mechanisms.

## 1. Introduction

In this work, we present a nacre-inspired material made from alumina platelets. Nacre, also known as mother of pearl, is the skeletal structure found in Gastropoda, Bivalvia and Cephalopoda mollusc shells, and is much stronger than any other mollusc shell structure independent of the type of loading [1]. Nacre is a ceramic/organic composite consisting of 95% aragonitic CaCO<sub>3</sub> and 5% organic material [2,3]. It consists of lamellar platelets approximately 0.5 µm thick [2,3] and 5–10 µm wide [4] arranged in a ‘brick-and-mortar’ structure in an organic matrix of 20–50 nm thickness [5].

A prominent role in the toughening of nacre, is thought to be energy dissipation through a platelet-platelet sliding process [6,7], which can be considered as an enlargement of the plastic zone. Ritchie et al. [4] point out that enlarging the plastic zone is an intrinsic toughening mechanism, effective against initiation and propagation of cracks. The existence of nano-asperities or surface roughness on the platelets has been argued to increase friction during sliding, but several studies have discounted this notion [8–10]. Instead, it is more likely that surface-waviness is a large contributor of surface friction [10,11]. Recently, Askarinejad et al. [12] have shown through both numerical and experimental analysis of platelets in a brick-and-mortar arrangement, that increasing platelet waviness increases the material stiffness, toughness and strength. Katti et al. [8] found that in a model without platelet

interlocking, nacre has a tensile strength of 14 MPa, while with platelet interlocking, nacre has a tensile strength of 50 MPa – a significant increase. Not all platelets in nacre seem to have this waviness though, as Barthelat et al. [10] observed both flat, regular and inverted dovetail structures in nacre. Nevertheless, the physical constraint against free movement of platelets that waviness can provide seems to be key to the strength and toughening of the nacre microstructure, suggesting that interlocking and accumulative pull-out of the platelets is the dominant toughening mechanism [7]. Lin and Meyers [2] show that another physical constraint seen in nacre suggested previously by Song et al. [13] can explain the high tensile strength values for nacre; the presence of the mineral bridges. Fan et al. [14] confirm Lin and Meyers’ views and conclude through a theoretical calculation that the mineral bridges effectively hinder crack extension. Another factor that comes into play in the sliding behaviour of nacre platelets, is platelet overlap. Both numeric [15] and experimental [12] efforts show that overlap of platelets is a main contributor to having simultaneous high strength and high toughness. From these studies it is clear that when the overlap length increases, the stiffness and strength of nacre improves.

Because of the unique mechanical properties of the ‘brick-and-mortar’ microstructure, alumina platelets similar in size to the CaCO<sub>3</sub> platelets found in nacre, have been of much interest in composite manufacturing. The flexural strength of individual alumina platelets has been measured to be 5.3 ± 1.3 GPa [16]. They have been compacted

\* Corresponding author.

E-mail address: [koen.evers@materials.ac.uk](mailto:koen.evers@materials.ac.uk) (K. Evers).<https://doi.org/10.1016/j.jeurceramsoc.2019.09.015>

Received 19 July 2019; Received in revised form 31 August 2019; Accepted 8 September 2019

Available online 09 September 2019

0955-2219/ © 2019 The Authors. Published by Elsevier Ltd. This is an open access article under the CC BY license (<http://creativecommons.org/licenses/by/4.0/>).

with epoxy [17,18], polymer [19–21], carbon nanotube [22], metallic [23] borosilicate [24] aluminium borate [25] and silica-calcia [26] phases. In this paper, we use these alumina platelets to template the grain structure of a pure alumina ceramic and investigate the mechanical behaviour of pure alumina with a nacre-like microstructure.

To effectively mimic the nacre microstructure, precise control over the grain growth while sintering the platelets into a dense ceramic is paramount. We therefore densified the alumina platelets using Spark Plasma Sintering (SPS), also known as Field-Assisted Sintering Technique (FAST). This technique enables us to sinter alumina in greatly reduced times compared to conventional hot-pressing and pressure-less sintering methods [27,28]. In addition to increased control over the grain size, the lower energy cost and relatively short timescale necessary to produce a sample makes SPS a very economic manufacturing route.

To investigate nacre-like microstructures using SPS, alumina platelets were sintered at different combinations of sintering temperature and pressure, thus generating a range of materials with distinct microstructural features, mainly in terms of size of the platelet-like grains. While SPS has not been systematically applied to powders of pure alumina platelets, the densification of alumina nanoparticles using SPS has been studied. Shen et al. [27] show that for alumina with a grain size of 0.4  $\mu\text{m}$ , fully dense samples can be obtained at 1150 °C in only 5 min. A later study by Santanach et al. [28] shows that for 0.14  $\mu\text{m}$  particles, full densification is obtained at temperatures of 1100 °C and higher. They see that in their experiments, grain growth only starts at 1200 °C, with significant grain growth at temperatures of 1300 °C and higher. Since alumina platelet powders have a grain size that is much larger, and since we must consider the poorer packing of platelet-powders, we have taken these temperatures as a lower bound. And have therefore densified at 1200 °C, 1300 °C and 1400 °C to see the effect on the microstructure and related mechanical properties.

Three-point bending tests were then carried out to characterise the mechanical behaviour of the manufactured materials. The different sintering conditions result in a range of nacre-like microstructures that as a result have varying flexural strengths. The material showing the most promising mechanical behaviour was selected for high-rate testing, first under compression using a split-Hopkinson bar apparatus, then upon impact of spherical steel projectiles. Direct comparison of the results of these tests for nacre-like and monolithic alumina specimens show strikingly different failure mechanisms, highlighting an enormous energy-absorbing capability of the manufactured nacre-like specimens.

## 2. Experimental

### 2.1. Ceramic manufacturing

15 g ( $\pm 1\%$ ) of  $\alpha$ -alumina platelets in powder form (RonaFlair® White Sapphire, MERCK, median diameter 8.4  $\mu\text{m}$ , width 0.2–0.5  $\mu\text{m}$ ), was loaded in a graphite die with an inner diameter of 40 mm and outer diameter of 80 mm. The powder was loaded without any de-agglomeration procedure to prevent contamination from dispersants and breakage of platelets in ball milling or other dispersion procedures. To protect the die and punches, the inside of the die and punches was lined with graphite paper (GEEGRAF flexible graphite foil, Gee Graphite). The sample was first pre-pressed using a hydraulic press to 15.5 MPa and then densified using a field assisted sintering technique (FAST) (Dr Fritsch Fast Sintering Press, FSP507) at temperatures between 1200 °C–1400 °C in vacuum (0.3 mbar) with a carbon felt insulation around the die. The temperature was measured at the wall of the die using a pyrometer. The dwell time was 15 min, with a heating rate of 125 °C/min. The pressure was increased linearly to either 50 or 70 MPa (maximum pressure for an intact graphite die) during heating and maintained at those levels during the entire dwell time. After the sintering process, the sample was cooled naturally without applied pressure to the die, which was measured to be 120 °C/min. The surface of

the discs was then ground to smooth the edges and remove residual graphite paper. A monolithic alumina specimen to compare impact and high-rate loading behaviour was sintered using 15 g alumina powder with a diameter of 0.4  $\mu\text{m}$  (AES11C, Sumitomo Chemical Co., Ltd.). The same sintering conditions were used as that of the best performing alumina-platelet sample; a dwell time of 15 min at 1300 °C and a 70 MPa sintering pressure, resulting in > 99% dense discs.

### 2.2. Characterisation

Density measurements were made using Archimedes' principle, by measuring dry, water-impregnated and water-submerged weights. The densities are then presented as a percentage of the theoretical density of  $\alpha$ - $\text{Al}_2\text{O}_3$ , 3.987 g/cm<sup>3</sup> [29]. Error bars represent variability in measured weights. For 3-point bend testing, the discs were polished and cut into 3.6  $\times$  2.7 mm rectangular beams using a diamond saw. For the impact tests and split Hopkinson pressure bar tests, the discs were polished and cut into 12 mm  $\times$  12 mm  $\times$  2.7 mm square plates and 3 mm  $\times$  3 mm  $\times$  2.7 mm squares respectively. After failure, the broken or impacted specimens were coated with 15 nm platinum and carefully transferred to a Zeiss Merlin high-resolution scanning electron microscope (SEM), equipped with an in-lens detector. To image the fracture surface from the three-point bend test, the specimen was coated again with 15 nm platinum after mounting upright and embedded in silver conductive paint to provide a conductive pathway for electrons and thus prevent charging effects. To show the grain boundaries in polished samples, the samples were thermally etched at 100 °C below the sintering temperature for 1.5 h. These thermally etched samples were then used to determine the grain width and length by measuring the distance from edge to edge of the grains (100 and 50 measurements per condition for grain width and length respectively).

### 2.3. Three-point bend testing

The 3.6  $\times$  2.7 mm rectangular beam specimens were subjected to a bend test in a Shimadzu loading frame with a 5 kN load cell. The loading frame was set-up with a three-point bend jig with a 20 mm span between outer rollers, and the cut specimens were loaded in the direction perpendicular to the orientation of the platelets with a stroke speed of 0.5 mm/min. The resulting force-deflection curves were then converted to stress-strain curves using standard formulae outlined in ASTM C1161-13.

### 2.4. Split Hopkinson pressure bar testing

The 3  $\times$  3 mm square specimens cut from the polished discs were tested under high-rate loading conditions using a split-Hopkinson compression bar. The compressive load was applied in the direction perpendicular to the orientation of the platelets (i.e. along the original disc thickness).

The split Hopkinson bar apparatus used consists of three aligned bars (i.e. projectile, input, and output bars) supported by low-friction polymeric circular bearings to avoid movement in the direction perpendicular to the bar axis. The projectile, accelerated using low-pressure compressed nitrogen, impacts the input bar generating a uniaxial stress pulse that travels along the bar and loads the specimen positioned between the input and the output bar.

The input and output bar, both with length of 2.8 m and diameter of 20 mm, are instrumented with strain gauges to measure the stress transmitted (output) and reflected (input) by the specimen, thus providing the information on the stress-strain behaviour of the tested material. The stress values are derived uniquely from the measures of the strain gauges on the bars, whilst the values of strain are corrected using Digital Image Correlation (DIC). Given the extremely small magnitude of the elastic deformation and the relative error in the DIC readings, small adjustments to the strain scaling have been made to

guarantee the consistency of the elastic behaviour.

In the tests presented in this work, disc anvils made of high-grade tungsten carbide (WC) were inserted between the ceramic specimen and the titanium (Ti6Al4V alloy) bars to prevent indentation of the metal. The correct sizing of the anvils (i.e. 10 mm diameter) ensures the impedance matching with the titanium bars, thus avoiding spurious signal reflection at the Ti6Al4V-WC interface. Further details of the apparatus used, and on the one-dimensional wave propagation analysis adopted can be found in works of De Cola [30] and Pellegrino [31].

The specimens were speckled with black paint and the tests were recorded using an ultra-high-speed camera (Kirana – Specialised Imaging Ltd.) with a frame rate of  $1 \cdot 10^6$  fps, for DIC purposes, and to provide visual evidence of the failure mechanisms exhibited by the materials.

## 2.5. Impact testing

The  $12 \times 12 \times 2.7$  mm square specimens cut from the polished discs were attached using a small layer of petroleum jelly to a flat aluminium surface, providing full backing support to the specimen, thus minimizing the occurrence of bending upon impact. The targets were impacted normally to the platelet orientation with spherical steel projectiles of 3 mm diameter. The steel projectiles were accelerated using a single stage gas gun, consisting of a pressurised vessel connected with a valve to a 2 m long barrel. At the opening of the valve, the compressed nitrogen released from the vessel accelerated the projectiles along the barrel. Three light gauges positioned at the end of the barrel measured the speed of the projectile before it impacted the surface of the target. Further details on the equipment used are provided in the work of Falco [32].

The impacts were recorded at an angle with a high-speed camera (FASTCAM SA5 – Photron), with a framerate of  $7.5 \cdot 10^4$  fps, to provide visual information on the crack initiation and propagation within the two materials upon impact. Depth measurements and the rendering of the impact crater were obtained using an Alicona infinite focus 3D profilometer microscope.

## 3. Results and discussion

### 3.1. Sintering and microstructure of nacre-like alumina

Alumina platelets were sintered at 1200 °C, 1300 °C and 1400 °C at a pressure of either 50 MPa or 70 MPa. The sintering curves in Fig. 1 give an indication of how well the samples were densified; no piston movement over long times is a good indication that the sample is not being densified further under the applied conditions. Both curves at

1200 °C stand out from curves at higher temperatures as they still show piston movement after half of the sintering time has elapsed, indicating a relatively poor density, which is confirmed by the density measurements in Fig. 1. The samples sintered at 1300 °C and 1400 °C show no more piston movement within 5 min of reaching the set sintering temperature, indicating maximum achievable density under their respective sintering conditions.

As expected, increased grain growth with increasing sintering temperature is observed (Figs. 2 and 3). While at 1200 °C the grain size is of the order of that of the initial platelet powder, at 1300 °C there is a wider grain size distribution, with both small and large grains co-existing (see also Fig. 4a). At 1400 °C the grains are an order of magnitude larger than that of the initial platelet powder. The effect of pressure when sintering alumina in SPS is normally to aid grain growth [33], but Fig. 3 shows that for all temperatures, both the grain width and length of the platelet-like grains is smaller at higher pressure. This is especially evident with the samples sintered at 1300 °C. We postulate that the increased pressure may play a role in breaking up agglomerates and the platelets themselves during sintering, resulting in smaller grains in the sintered alumina.

The tendency of platelets to align naturally has been shown before in a sedimentation procedure [34]. The pre-pressing procedure combined with the (platelet) particle rearrangement/sliding [35] during sintering under the applied pressure is likely responsible for the observed large scale-alignment of platelets (and consequently platelet-like grains).

Interestingly, the platelet-like morphology of the grains is maintained at all temperatures regardless of grain growth, although the aspect ratio of the platelet-like grains reduces with increased temperature. After platelets combine to larger platelet-like grains, Fig. 4c shows that these are often not monocrystalline domains, and nano-sized voids are present within the platelet structure. While it is possible that slightly misaligned domains and pores may already have existed in the alumina platelet powder, we note that the platelets in the starting powder (Fig. 4d) likely grow not only by classical grain boundary migration, but also by the coalescence of neighbouring platelets. This is presumed to be a consequence of the fact that the crystallographic c-axis [001] is normal to plane of the platelets [36]. The physical alignment of the platelets (Fig. 4a,b) in these composites therefore also corresponds to a crystallographic alignment, opening the possibility of grain coalescence. It is also possible that local plastic deformation occurs around mis-stacked platelets during SPS, creating dislocations, which then form subgrains via recovery. Fig. 4b further shows that the grain growth leads to the formation of platelets with irregular ‘wavy’ shapes. The ‘steps’ that are formed can be seen to interlock in a similar manner as described for nacre by Katti *et al* [37].

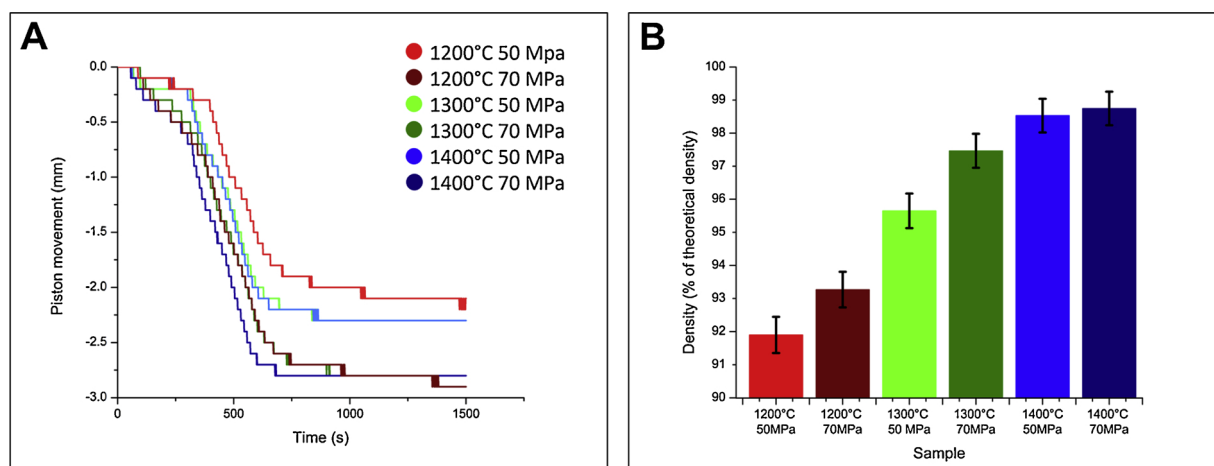
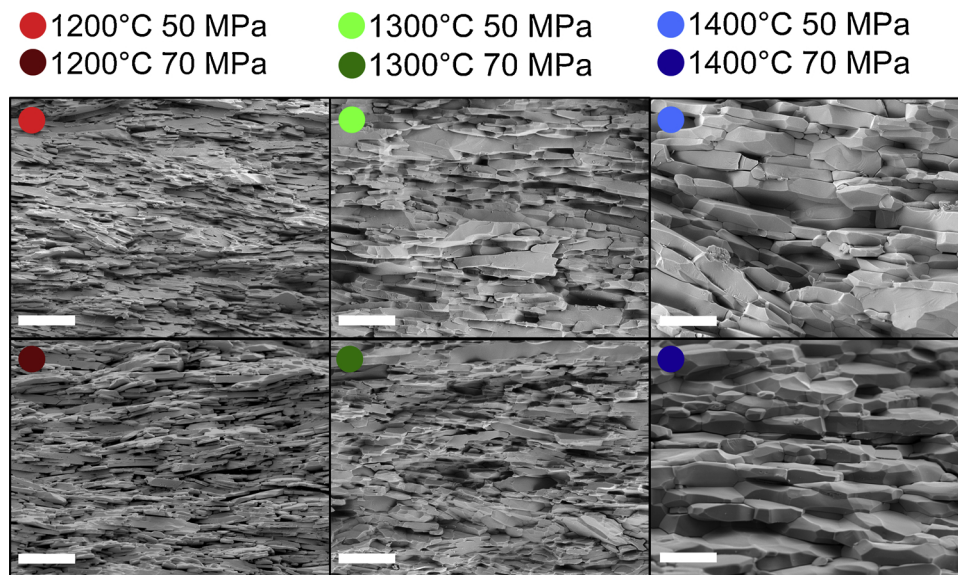
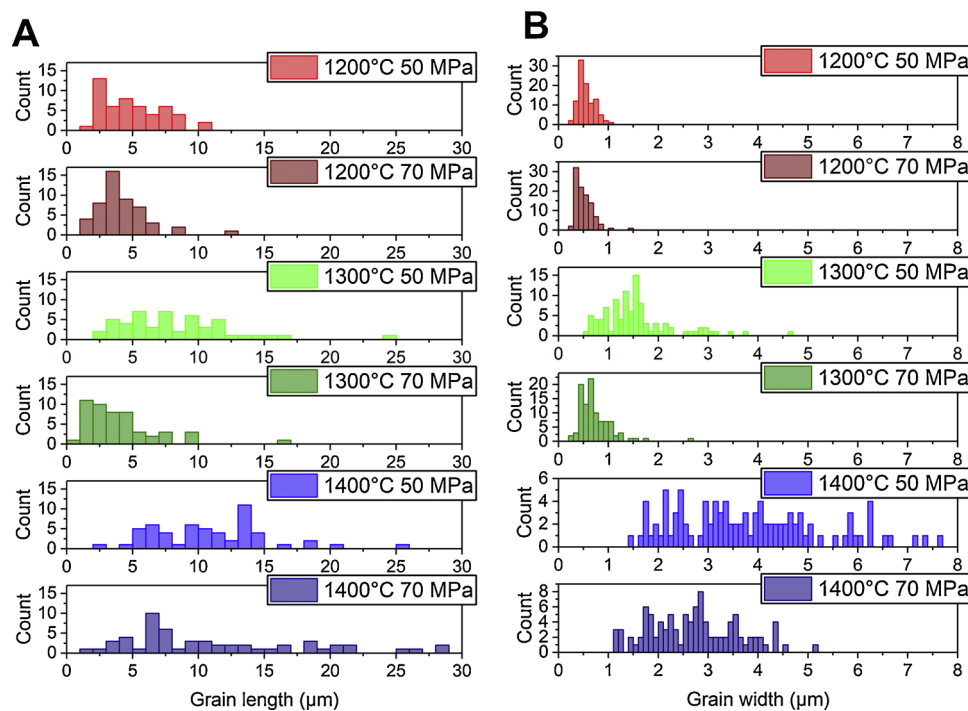


Fig. 1. a) Sintering curves for each sintering condition showing piston movement in FAST and b) their densities after sintering.



**Fig. 2.** SEM micrographs taken of the fracture surface of the beams after bend testing, showing coarser platelet-like grains with increasing sintering temperature. Scalebars: 10  $\mu\text{m}$ .



**Fig. 3.** a) Measurements of grain length (bin size: 1  $\mu\text{m}$ ) and b) grain width (bin size: 0.1  $\mu\text{m}$ ) of platelet-like grains for all used sintering conditions. For all grain size measurements taken at the same sintering temperature, a higher number of smaller grains are observed at higher pressures.

### 3.2. Mechanical response in bending

In three-point bending, we observe that nacre-like alumina does not fail in a purely brittle fashion with a macroscopically flat fracture surface as is normally observed for monolithic alumina. Instead all samples, regardless of grain size, show evidence of crack deflection and branching as seen in nacre (Fig. 5).

The tortuous and thus prolonged crack paths along the platelets result in macroscopic interlocking after failure which gives the material post-failure load bearing capabilities seen in Fig. 6. Due to being interlocked both macroscopically and microscopically, the beams stay suspended on the rollers of the bending rig after failing. The beams stay so connected that they can easily be transferred without falling apart,

which is very rare for a pure ceramic specimen after failure.

Samples sintered at 1200  $^{\circ}\text{C}$  have comparatively low density and resulting low flexural strength values between 54–96 MPa - the platelets compacted with minimal grain growth occurring, but also with minimal bonding. Sintering at 1300  $^{\circ}\text{C}$  yielded a higher density material (Fig. 1) with a wider grain-size distribution. The samples which were sintered at 1300  $^{\circ}\text{C}$  have much higher flexural strength values, with the sample sintered at 70 MPa exhibiting flexural strengths of 120–150 MPa. These samples also possessed the greatest residual strength of up to 30 MPa after the initial fracture event. We believe the observed mechanical improvements are due to an increased bonding between platelets, which leads to increased friction during platelet-platelet sliding [2,13,14], while at the same time maintaining relatively small platelet

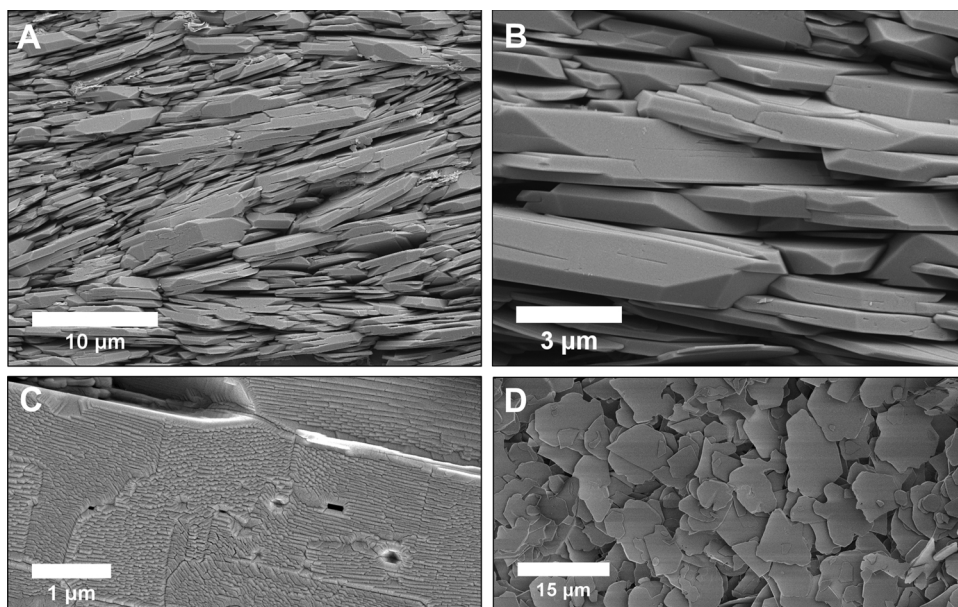


**Fig. 4.** SEM micrographs taken of a–c) the side of the beams sintered at 1300 °C, and d) the platelet-alumina powder that was loaded into the graphite die to create the nacre-like alumina. We show that a) starting at 1300 °C, a number of platelets nucleate grain growth and form larger platelets, resulting in a wider grain size distribution. b) Larger grains are shown to be formed by bonding platelets with similar dimension and orientation. c) The thermally etched, polished surface shows the grain or sub-grain boundaries within the platelet-like grains and associated nano-sized voids in the platelet structure.

dimensions in a large fraction of the bulk.

Fig. 7 shows that the formation of larger, more irregularly shaped platelets also increases average platelet waviness [8] and platelet diameter resulting in a greater bridging and pull-out length. Fig. 8 shows that these platelet-like grains promote crack deflection and bridging, causing interlocks during crack propagation which restrain the crack faces and toughen the material. The interlocks often cause the crack to branch resulting in a diffuse fracture. The platelet-platelet interlocking is further promoted by the fact that while the platelets are aligned, it is not uncommon for platelets to be slightly tilted with respect to one another. The existence of platelet-like grains with cracks all around them further demonstrates the interlocking behaviour.

Sintering at 1400 °C decreases the strength, which we attribute to the prevalent grain growth shown in Fig. 2 and 3 – The platelet-character of the grains is diminished, and the increased grain size can also lead to an increase in the size of pre-existing microcracks which is detrimental for material strength [38].

We note however that for alumina platelets sintered at higher temperatures, it is possible to improve the flexural strength by modifying processing parameters such as the heating and cooling rates, dwell time and time of pressure application. These parameters can affect the plastic deformation of the platelets, grain growth, critical defect size and therefore the strength. For example, we have previously reported platelet-like alumina sintered using SPS at 1600 °C and 45 MPa with a flexural strength of around ~180 MPa [22]. In addition, alumina platelets sintered with alumina nanoparticle additions [25,26] sintered

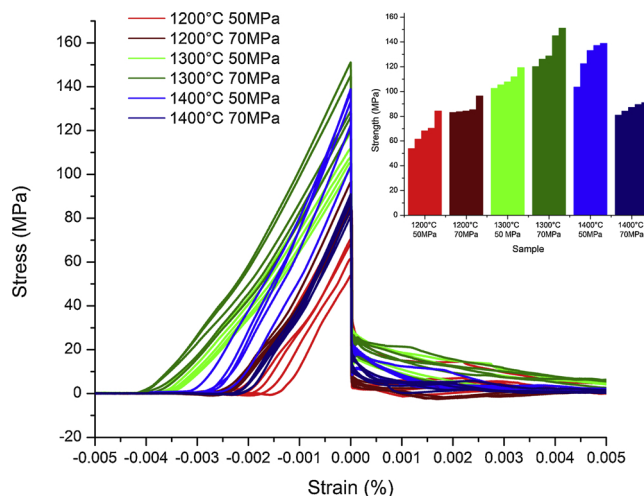


**Fig. 6.** Three-point bending stress-strain curves from samples sintered under different temperatures and pressures, with the strengths reported separately in the inset. The curves are plotted with the point of failure set at zero strain to visualize and quantify the accommodated strain.

at temperatures above 1400 °C have shown to be able to yield alumina with a flexural strength around ~300 MPa [25,26]. We are confident therefore that the processing can be further refined to yield higher

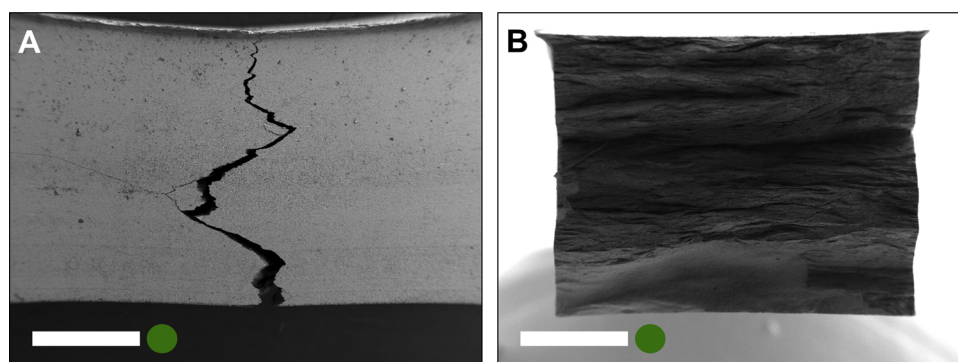


**Fig. 5.** SEM micrograph of a) the side-view of the beam sintered at 1300 °C and 70 MPa after it has failed in 3 pt bend testing, and b) its corresponding fracture surface (with the conductive silver paint pathway at the bottom). Scalebars: 1 mm.

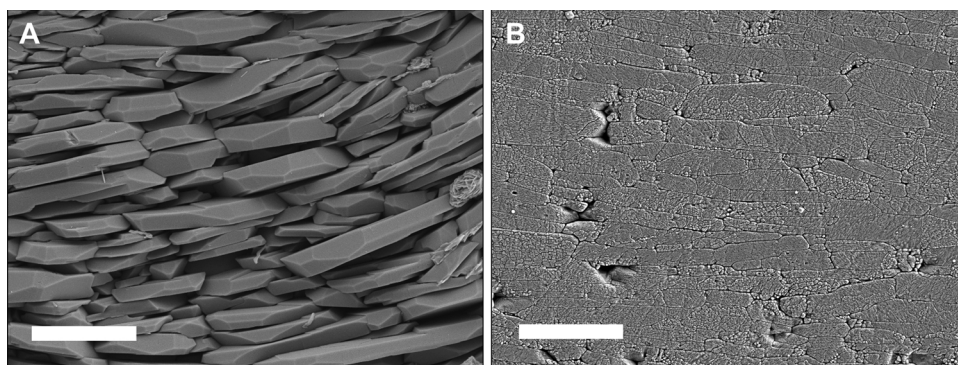


**Fig. 7.** SEM micrographs taken of the side of the beam sintered at 1300 °C and 70 MPa, showing enlarged platelet-like grains a) after cutting before polishing and thermal etching and b) after polishing and thermal etching. The platelet-like grains have differing sizes and their irregular shape displays 'waviness', promoting interlocking during crack propagation. Scalebars: 5 µm.

strengths. However, for pure alumina specimens, the nacre-like character of the alumina grains in materials sintered at these temperatures is drastically reduced due to grain growth, as shown in Fig. 3. It has been demonstrated that creating composites using alumina platelets can be a solution to inhibit grain growth able to improve the flexural strength of the material while largely maintaining the size of the platelets [23,25,26]. For pure nacre-like alumina examined here, the material sintered at 1300 °C and 70 MPa, which shows both small platelet-like grains and the highest flexural strength of all manufactured samples, was selected for dynamic testing.

### 3.3. Mechanical response under dynamic loading

The material exhibiting the highest values of strength and strain to failure (i.e. sintered at 1300 °C and 70 MPa) was tested under dynamic loading conditions, alongside monolithic alumina, to explore the effect of the platelet-like grains on the high strain rate behaviour of the material.

Split-Hopkinson compression bar tests were carried out on three specimens for each of the two materials considered, imposing the same loading conditions, which resulted in a strain-rate of the order of  $500 \pm 100 \text{ s}^{-1}$ . The results are summarised in the stress-strain curves reported in Fig. 9.

The stress-strain curves of the monolithic alumina (solid lines) show a typical brittle behaviour, with elastic deformation followed by sudden failure of the whole specimen. Additionally, the analysis of the high-speed camera images of the tests reported shows the sudden and complete failure of the specimens at the onset of damage.

The stress-strain curves of the nacre-like alumina instead show a noticeably higher strength. Additionally, the final part of the stress-strain curves shows the ability of the nacre-type alumina to continue to carry load following the onset of damage before the complete failure of the material. In this test one of the specimens, despite developing internal cracks, survived the compression test without failing. This

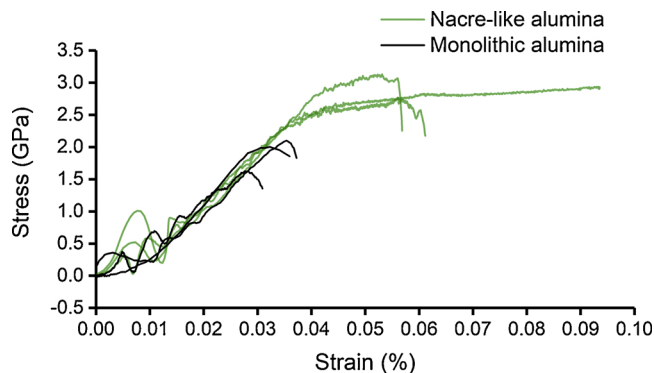


**Fig. 9.** Comparison of the mechanical behaviour of monolithic and nacre-like alumina under dynamic compression.

specimen is represented by the longest curve in Fig. 9.

From these tests, it is evident that the presence of platelet-like grains increases the high-rate compressive strength with respect to the monolithic material significantly as well as providing an inelastic deformation plateau in lieu of the usual sudden brittle failure of monolithic alumina. This behaviour can be explained by the presence of the crack deflection and crack branching mechanisms described in the previous section.

Visual evidence of the behaviour described can be obtained from the high-speed camera recording presented in Fig. 10, showing the different failure mechanisms. Whilst the monolithic alumina (top row) exhibits a uniform and brittle failure, the nacre-like specimen (bottom row) shows a much more gradual failure, with the cracks initiating at the bottom of the specimen and spreading throughout the domain, thus delaying the occurrence of the final failure.

The measured stress-strain curves and the direct observation of the failure of the specimens, provide evidence of the occurrence of the

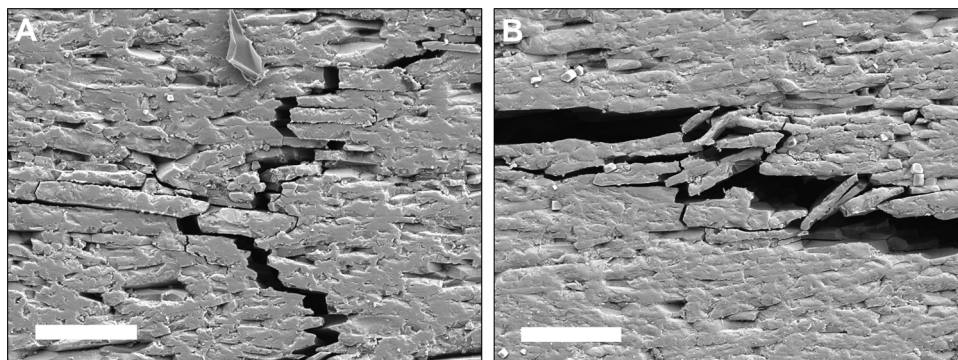


**Fig. 8.** SEM micrographs of a side-view of the beam after three-point bend testing, showing typical crack propagation a) across the alumina and b) along the alumina. Scalebars: 10 µm.

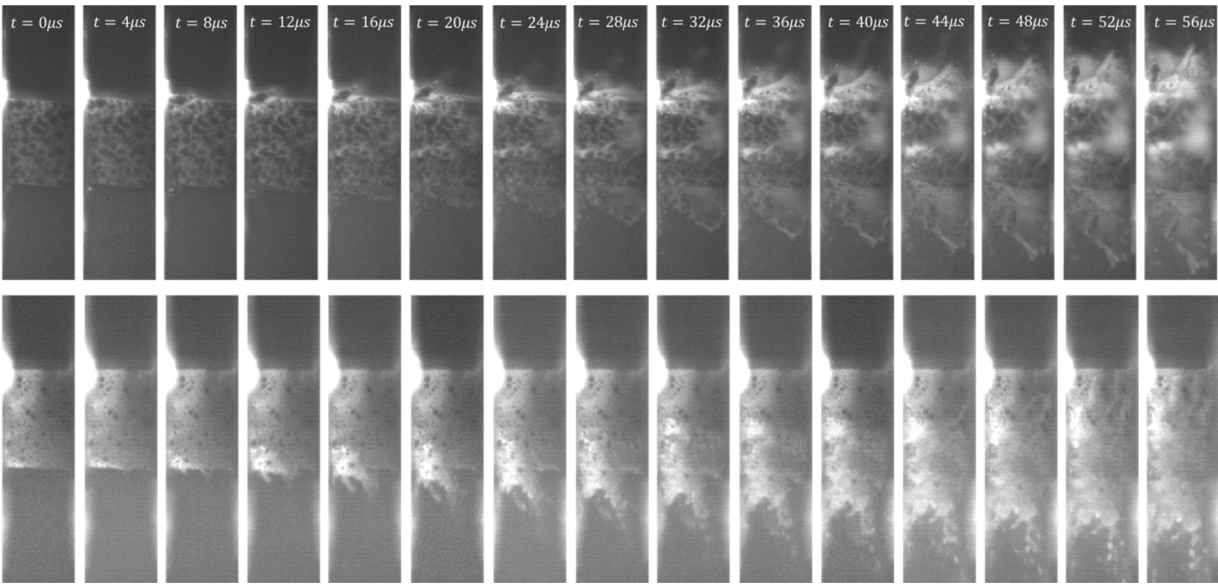


Fig. 10. Failure mechanisms of monolithic (top) and nacre-like (bottom) alumina under high strain rate compression.

Table 1

An overview of the impact velocities, calculated kinetic energy of the projectile and resulting post-mortem visual analysis of specimens after impact-testing, showing a clear improvement in performance provided by the nacre-like alumina.

	Impact velocity [m/s]	Kinetic energy [J]	Post-mortem status
Monolithic alumina	136	1.05	Intact
	150	1.28	Broken
	179	1.82	Broken
	207	2.44	Broken
Nacre-like alumina	204	2.37	Diffuse cracks
	215	2.63	Diffuse cracks
	253	3.64	Diffuse cracks
	272	4.21	Diffuse cracks

crack deflection mechanism in the nacre-like alumina also during split-Hopkinson bar compression tests. The results of these tests show that nacre-like alumina has improved performance over monolithic alumina also at high strain rates.

3.4. Mechanical response upon impact

To verify the effect of the crack-deflection mechanism observed for high-rate compression, the nacre-like alumina was also tested upon impact at different velocities. The results of the tests carried out on both monolithic and nacre-like alumina are reported in Table 1, showing a clear improvement in performance provided by the crack-deflection mechanism observed in the other tests presented.

The presence of platelet-like grains makes the material capable of withstanding impact velocities substantially higher than monolithic alumina by absorbing the energy via the propagation of diffuse cracks within the domain. In contrast with monolithic or even armour-grade alumina materials where specimens have to be laterally constrained to prevent alumina from falling apart after impact [39], the nacre-like alumina presented in this work is able to sustain extensive cracking without compromising the overall structural integrity of the specimen.

Fig. 11 reports the visual comparison of the impact of a steel spherical projectile on the monolithic (top row) and nacre-like (bottom row) alumina, with impact velocities equal to 207 m/s and 204 m/s, respectively. The different energy absorption mechanisms leading to the contrasting performances of the materials can be clearly observed.

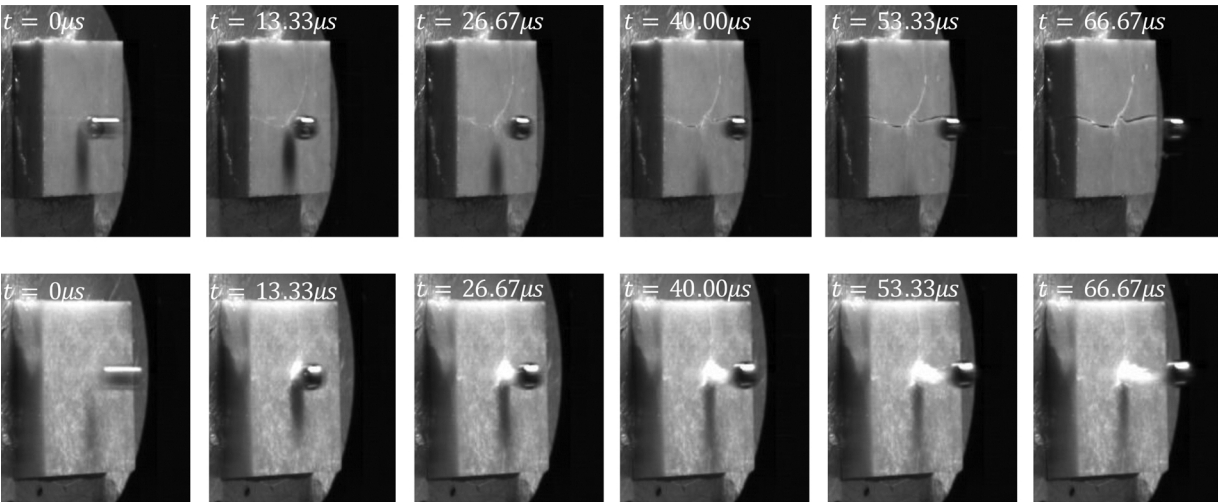


Fig. 11. Impact of a steel sphere against monolithic (top) and nacre-like (bottom) alumina.

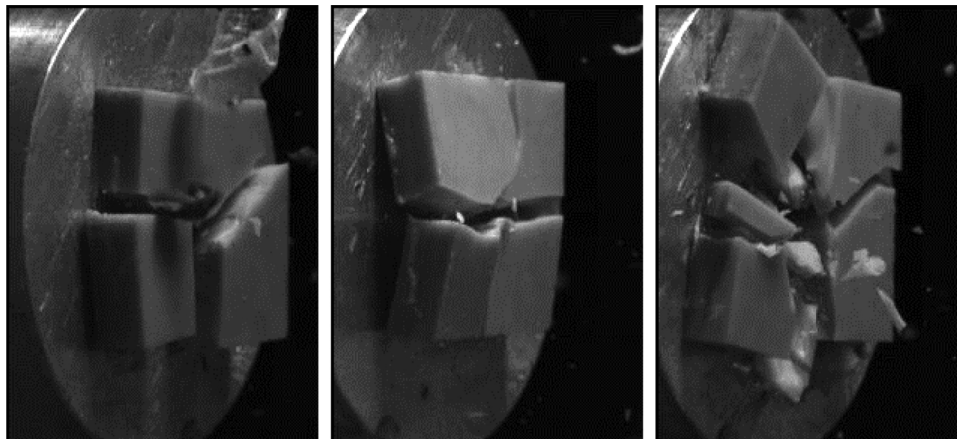


Fig. 12. Post-impact fragmentation of monolithic alumina targets.

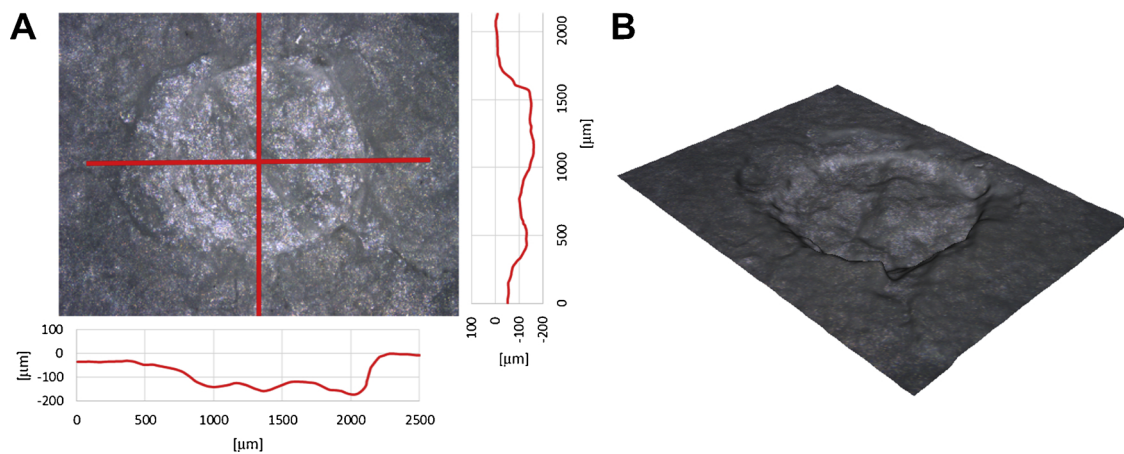


Fig. 13. a) Profilometry after impact on nacre-like alumina and b) 3D reconstruction of the impact crater (right).

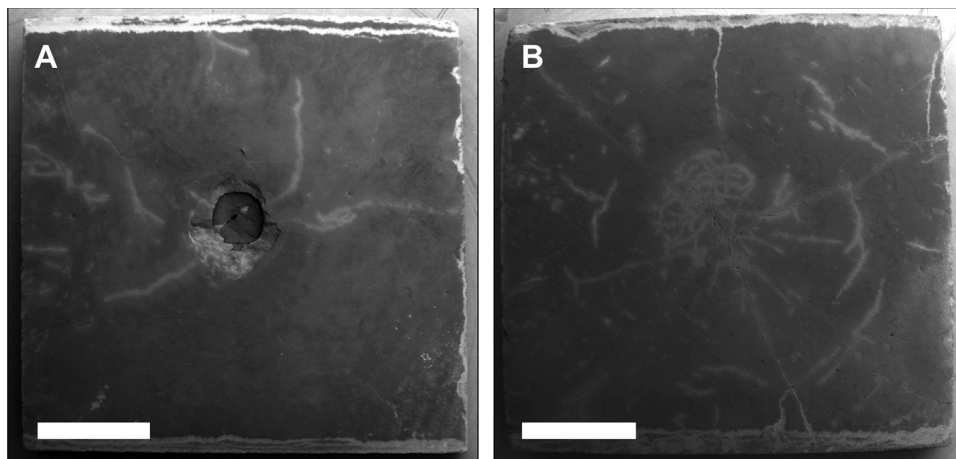


Fig. 14. SEM micrographs of a) the front and b) the back of the nacre-like alumina target, showing the net of radial cracks propagating from the impact point throughout the whole domain. Scalebars: 3 mm.

In the monolithic alumina 4 radial cracks propagate from the impact area, leading to the rapid and complete failure of the specimen. Example of the extent of the failure of the monolithic alumina specimens is given by the high-speed camera frames in Fig. 12. The post-impact images show the extreme fragmentation of the target tiles.

The nacre-like alumina, on the contrary, remained intact. The growth of a higher number of diffuse cracks radiating and branching from the impact area indicates a more uniform spread of the damage

within the whole volume. Additionally, the projectile causes pulverisation of the target at the contact point (clearly visible in the images presented) leading to the formation of an impact crater.

The profilometry and the 3D reconstruction of the impact zone, for the test on nacre-like alumina impacted at a velocity of 253 m/s, is reported in Fig. 13. Analysis of the 3D reconstruction of the impact area shows the formation of a crater, measuring almost 0.15 mm in depth and 1.5 mm in diameter.

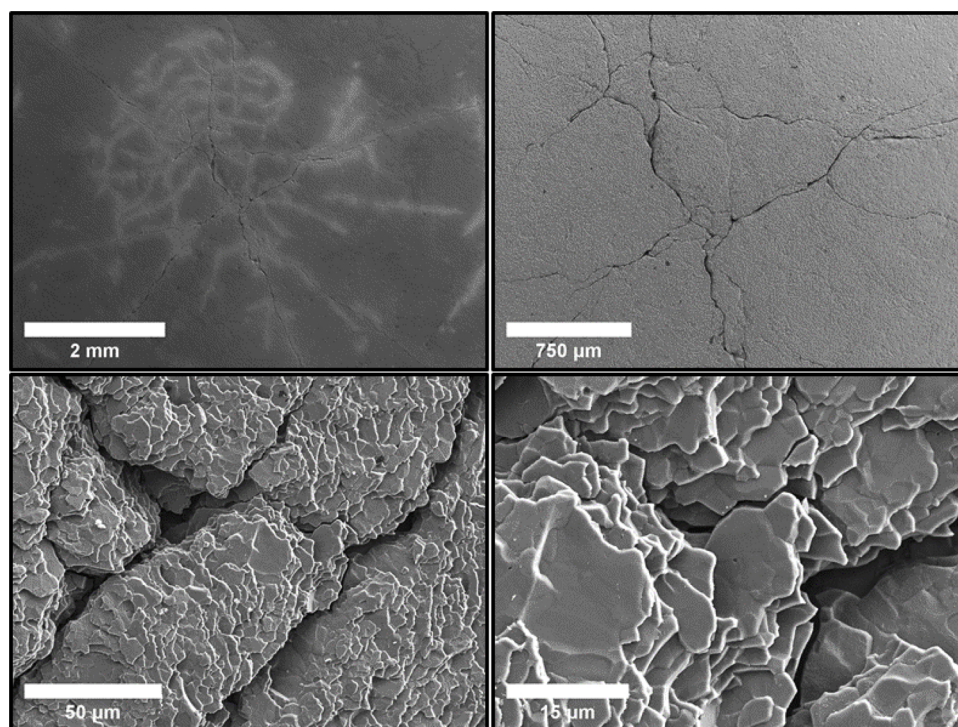


Fig. 15. SEM micrographs showing a zoom-in of the back-face cracks at the impact point.

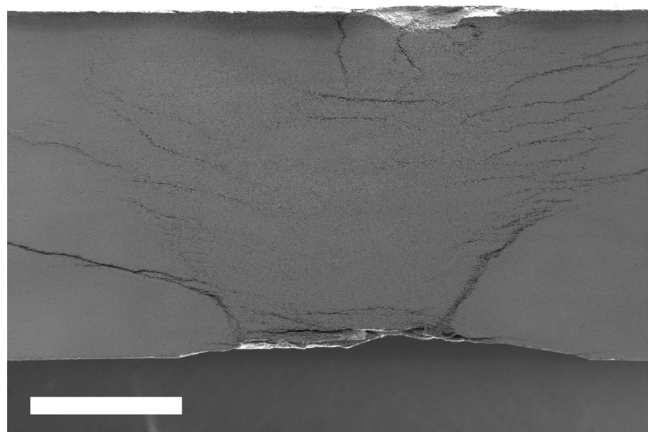


Fig. 16. SEM micrograph showing a cross-section of the impact crater (bottom of the image), revealing large outward crack deflection. Scalebar: 1mm.

The extension of the cracks propagating from the impact crater can be observed in the SEM images shown in Fig. 14. The missing chip of material along the bottom of the crater (still visible in Fig. 13) was lost during the preparation of the specimen (i.e. blowing off contaminants from the impact test using compressed air) prior to SEM. Additionally, the back face of the target also shows an extensive net of cracks propagating from the impact point. Despite the wide extent of the propagation of cracks, the specimen maintains its structural integrity. Maintaining structural integrity after impact is an important feature for the multi-hit capability of the material; it has been shown that cracks in alumina ballistic armour have a negligible effect on performance as long as structural integrity is maintained [40].

A detail of the cracks developing along the back surface is presented in Fig. 15, showing the presence of the deflection mechanism more clearly. The dispersion of kinetic energy through the deflection of cracks leads to the improvement in performance of nacre-like alumina over the monolithic material. It is also worth noticing that these materials are tested without confining them as is commonly done for

ballistic tests, where confinement has been shown to dramatically increase compressive strength [41].

To visualize the deflection mechanism throughout the thickness of the impact specimen, a cross section at the impact crater is presented in Fig. 16. Cracking is deflected and dispersed outward into the alumina. This is especially clear when considering the Hertzian cone-crack which is deflected into multiple lateral cracks which propagate along the platelet-like grains.

#### 4. Conclusions

Micron-sized alumina platelet powders have been used to generate nacre-like alumina with different grain sizes. The mechanical behaviour of nacre-like alumina manufactured at different temperatures and pressures has been correlated to their microstructures. We show that we can maintain nacre-like aligned platelet-grains while achieving a dense ceramic by using SPS and show that this results in specimens with radically different fracture behaviour. The main feature of these materials is that due to interlocking platelets and crack deflection, the material stays intact with internal cracking instead of breaking destructively as monolithic alumina does. This is especially evident in impact testing of these materials, where even after a four times kinetic energy-increase of the projectile, the specimen did not fail, and only diffuse cracks were observed. This reflects a tendency for cracks to deflect along a direction parallel to the platelets. When these materials were tested in dynamic loading conditions, they show significant improvement over monolithic alumina both in terms of strength and accommodated strain.

#### Acknowledgements

We would like to thank Jeffrey Fullerton and Radka Chakalova for their help with cutting our ceramic specimens. We are grateful to Professor Patrick Grant for allowing us access to his Fast Sintering Press in the Advanced Processing Laboratory and Professor Nik Petrinic for allowing us the use of high rate testing equipment in the Impact Engineering Laboratory. We are grateful for the financial support from the Royal Society (N.G.), the European Research Council; ERC-2009-

StG-240500-DEDIGROWTH; ERC-2011-PoC-309786-DEVICE; ERC-2015-PoC-680559 – CONDUCT; ERC-2016-PoC-754748-OxfordNano (N.G.), the Engineering and Physical Sciences Research Council and the US Army Engineer Research and Development Center.

## References

- [1] J.D.D. Currey, Mechanical properties of mother of Pearl in tension, *Proc. R. Soc. B Biol. Sci.* 196 (2001) 19–20.
- [2] M.A. Meyers, A.Y.M. Lin, P.Y. Chen, J. Muyco, Mechanical strength of abalone nacre: role of the soft organic layer, *J. Mech. Behav. Biomed. Mater.* 1 (2008) 76–85.
- [3] R. Menig, M.H. Meyers, M.A. Meyers, K.S. Vecchio, Quasi-static and dynamic mechanical response of *Haliotis rufescens* (abalone) shells, *Acta Mater.* 48 (2000) 2383–2398.
- [4] R.O. Ritchie, The conflicts between strength and toughness, *Nat. Mater.* 10 (2011) 817–822.
- [5] F.D. Fleischli, M. Dietiker, C. Borgia, R. Spolenak, The influence of internal length scales on mechanical properties in natural nanocomposites: a comparative study on inner layers of seashells, *Acta Biomater.* 4 (2008) 1694–1706.
- [6] R. Rabiei, S. Bekah, F. Barthelat, Failure mode transition in nacre and bone-like materials, *Acta Biomater.* 6 (2010) 4081–4089.
- [7] H. Kakisawa, T. Sumitomo, The toughening mechanism of nacre and structural materials inspired by nacre, *Sci. Technol. Adv. Mater.* 12 (2011) 064710.
- [8] K.S. Katti, D.R. Katti, Why is nacre so tough and strong? *Mater. Sci. Eng. C* 26 (2006) 1317–1324.
- [9] D.R. Katti, S.M. Pradhan, K.S. Katti, Modeling the organic-inorganic interfacial nanoasperities in a model bio-nanocomposite, nacre, *Rev. Adv. Mater. Sci.* 6 (2004) 162–168.
- [10] F. Barthelat, H. Tang, P.D. Zavattieri, C.M. Li, H.D. Espinosa, On the mechanics of mother-of-pearl: a key feature in the material hierarchical structure, *J. Mech. Phys. Solids* 55 (2007) 306–337.
- [11] F. Barthelat, H.D. Espinosa, An experimental investigation of deformation and fracture of nacre-mother of pearl, *Exp. Mech.* 47 (2007) 311–324.
- [12] S. Askarinejad, H.A. Choshali, C. Flavin, N. Rahbar, Effects of tablet waviness on the mechanical response of architected multilayered materials: modeling and experiment, *Compos. Struct.* 195 (2018) 118–125.
- [13] F. Song, Y.L. Bai, Effects of nanostructures on the fracture strength of the, *J. Mater. Res.* 18 (2003) 1741–1744.
- [14] B. Yilong, S. Fan, Mineral bridges of nacre and its effects, *Acta Mech. Sin.* 17 (2001) 251–257.
- [15] X. Wei, M. Naraghi, H.D. Espinosa, Optimal length scales emerging from shear load transfer in natural materials: Application to carbon-based nanocomposite design, *ACS Nano* 6 (2012) 2333–2344.
- [16] E. Feilden, et al., Micromechanical strength of individual Al<sub>2</sub>O<sub>3</sub>platelets, *Scr. Mater.* 131 (2017) 55–58.
- [17] D.K. Shukla, V. Parameswaran, Epoxy composites with 200 nm thick alumina platelets as reinforcements, *J. Mater. Sci.* 42 (2007) 5964–5972.
- [18] D.K. Shukla, S.V. Kasisomayajula, V. Parameswaran, Epoxy composites using functionalized alumina platelets as reinforcements, *Compos. Sci. Technol.* 68 (2008) 3055–3063.
- [19] R.M. Erb, R. Libanori, N. Rothfuchs, A.R. Studart, Composites reinforced in three dimensions by using low magnetic fields, *Science* 202508 (2012) 199–204.
- [20] M. Petrini, M. Ferrante, B. Su, Fabrication and characterization of biomimetic ceramic/polymer composite materials for dental restoration, *Dent. Mater.* 29 (2013) 375–381.
- [21] P. Song, et al., Thermally stable, conductive and flame-retardant nylon 612 composites created by adding two-dimensional alumina platelets, *Compos. Part A Appl. Sci. Manuf.* 97 (2017) 100–110.
- [22] K. Evers, H. Porwal, R.I. Todd, N. Grobert, MWCNT-coated alumina micro-platelets for nacre-like biomimetic composites, *Carbon* 145 (2019) 586–595.
- [23] H. Le Ferrand, F. Bouville, T.P. Niebel, A.R. Studart, Magnetically assisted slip casting of bioinspired heterogeneous composites, *Nat. Mater.* 14 (2015) 1172–1179.
- [24] P. Šandera, et al., Toughening effects quantification in glass matrix composite reinforced by alumina platelets, *Acta Mater.* 56 (2008) 2908–2918.
- [25] P.I.B.G.B. Pelissari, et al., Nacre-like ceramic refractories for high temperature applications, *J. Eur. Ceram. Soc.* 38 (2017) 2186–2193.
- [26] F. Bouville, et al., Strong, tough and stiff bioinspired ceramics from brittle constituents, *Nat. Mater.* 13 (2014) 508–514.
- [27] Z. Shen, M. Johansson, Z. Zhao, M. Nygren, Spark plasma sintering of alumina, *J. Am. Ceram. Soc.* 27 (2002) 1921–1927.
- [28] J.G. Santanach, et al., Spark plasma sintering of alumina: study of parameters, formal sintering analysis and hypotheses on the mechanism(s) involved in densification and grain growth, *Acta Mater.* 59 (2011) 1400–1408.
- [29] D.L. Perry, *Handbook of Inorganic Compounds*, CRC Press, 2011.
- [30] F. De Cola, A. Pellegrino, E. Barbieri, D. Penumadu, Void ratio based representative volume element for modelling the high strain rate behaviour of granular materials, *Int. J. Impact Eng.* 91 (2016) 46–55.
- [31] A. Pellegrino, A. Wear, The dynamic response of etnean sand and the effect of its impingement on Ti-6Al-4 V alloy, *J. Dyn. Behav. Mater.* 2 (2016) 438–451.
- [32] S. Falco, *Numerical Modelling and Experimental Characterisation of Mechanical Performance of Ceramic Materials at Multiple Scales*, University of Oxford, 2015.
- [33] B. Ratzker, A. Wagner, M. Sokol, S. Kalabukhov, N. Frage, Stress-enhanced dynamic grain growth during high-pressure spark plasma sintering of alumina, *Acta Mater.* 164 (2019) 390–399.
- [34] S. Behr, U. Vainio, M. Müller, A. Schreyer, Ga. Schneider, Large-scale parallel alignment of platelet-shaped particles through gravitational sedimentation, *Sci. Rep.* 5 (2015) 9984.
- [35] R. Chaim, *Grain Growth During Spark Plasma and Flash Sintering of Ceramic Nanoparticles: a Review*, (2018), pp. 3087–3105, <https://doi.org/10.1007/s10853-017-1761-7>.
- [36] A.S. Sokolov, V.G. Harris, 3D crystallographic alignment of alumina ceramics by application of low magnetic fields, *J. Eur. Ceram. Soc.* 38 (2018) 5257–5263.
- [37] K.S. Katti, D.R. Katti, S.M. Pradhan, A. Bhosle, Platelet interlocks are the key to toughness and strength in nacre, *J. Mater. Res.* 20 (2005) 1097–1100.
- [38] M.E. Launey, R.O. Ritchie, On the fracture toughness of advanced materials, *Adv. Mater.* 21 (2009) 2103–2110.
- [39] B.G. Compton, E.A. Gamble, F.W. Zok, Failure initiation during impact of metal spheres onto ceramic targets, *Int. J. Impact Eng.* 55 (2013) 11–23.
- [40] I. Horsfall, D. Buckley, The effect of through-thickness cracks on the ballistic performance of ceramic armour systems, *Int. J. Impact Engng* 18 (1996) 309–318.
- [41] J. Lankford Jr., The role of dynamic material properties in the performance of ceramic armor, *Int. J. Appl. Ceram. Technol* 10 (2004) 205–210.